ACS Photonics

Article

pubs.acs.org/journal/apchd5

Optimum Forward Light Scattering by Spherical and Spheroidal Dielectric Nanoparticles with High Refractive Index

Boris S. Luk'yanchuk,*[,†,‡] Nikolai V. Voshchinnikov,[§] Ramón Paniagua-Domínguez,[†] and Arseniy I. Kuznetsov[†]

[†]Data Storage Institute, A*STAR (Agency for Science, Technology and Research), 5 Engineering Drive 1, 117608, Singapore

[‡]School of Electrical and Electronic Engineering, Nanyang Technological University, 639798 Singapore

[§]Sobolev Astronomical Institute, Saint Petersburg University, Saint Petersburg, 198504, Russia

Supporting Information

ABSTRACT: High-refractive index dielectric nanoparticles may exhibit strong directional forward light scattering at visible and near-infrared wavelengths due to interference of simultaneously excited electric and magnetic dipole resonances. For a spherical particle shape, the so-called first Kerker's condition can be realized, at which the backward scattering practically vanishes for some combination of refractive index and particle size. However, realization of Kerker's condition for spherical particles is only possible at the tail of the scattering resonances, when the particle scatters light weakly. Here we demonstrate that significantly higher forward scattering can be realized if spheroidal particles are considered instead. For each value of refractive index n exists an optimum shape of the particle, which produces minimum backscattering efficiency together with maximum forward scattering. This effect is achieved due to the overlapping of magnetic and electric dipole resonances of the spheroidal particle at the resonance frequency. It permits the design of very efficient, low-loss optical nanoantennas. We show that the results obtained for spheroidal particles can accurately describe the response of a wide range of practical particle shapes with the same aspect ratio, which can be obtained in experiment.

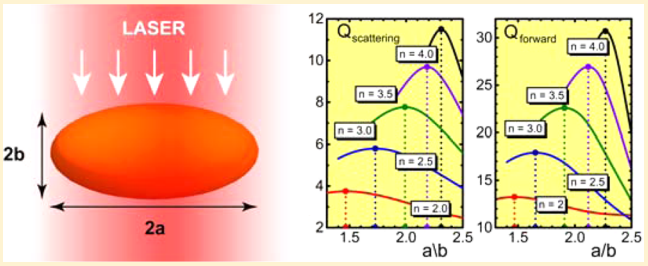

KEYWORDS: *high-index dielectric nanoparticles, Mie resonances, forward light scattering, Kerker's condition, spheroidal particles, nanoantennas*

Resonant nanoparticles and nanoantennas[1] become crucially important for advanced photonic technologies including on-chip interconnects, bioimaging, solar-cells, heat-assisted magnetic recording, and so on. They can play the role of nanooptical elements, which may substitute conventional optics at subwavelength scale. During the past few years significant attention has been paid to nanoparticles made of low-loss high-refractive index dielectric and semiconductor materials, in which one can observe both electric and magnetic dipole resonances with comparable strengths at optical frequencies.[2−8] Interference of these two modes allows to fulfill a condition for almost zero backward light scattering, as proposed by Kerker et al. for spherical particles more than three decades ago.[9,10] Thus, these materials open a fascinating opportunity to control directionality of scattering and design efficient low-loss nanoantennas.[11−13] The Kerker's-type directional scattering was experimentally demonstrated first for millimeter-scale ceramic spheres in the microwave regime,[14] and shortly after for nanometer-scales silicon nanospheres[15] and gallium arsenide nanodisks[16] in the visible spectral range.

In all the above cases, the zero-backward scattering condition has been fulfilled on the long-wavelength tail of the magnetic dipole resonance out of the maximum of the scattering amplitude. However, it was shown recently that, for nanostructures with nonspherical shape, namely, flat silicon disks with an aspect ratio around 1:2, electric and magnetic dipole resonances can be overlapped,[17] providing a strong forward scattering and almost zero backward scattering at the scattering resonance maximum.

In this paper, we demonstrate that for spheroidal nanoparticles one can always find an optimum aspect ratio, at which the overlapped electric and magnetic dipole resonances provide simultaneously minimal backscattering and optimized forward scattering. This optimum shape depends on the specific value of material refractive index. We work in the frame of exact light scattering methods and consider spheres and spheroids with different aspect ratios.

First, scattering properties of spherical nanoparticles have been analyzed using Mie theory[18] (see Methods for details). Figure 1 presents different scattering characteristics of spherical nanoparticles with radius R versus their refractive index n and size parameter $q = 2\pi R/\lambda$ (here λ is the wavelength of incident light). In particular, the partial scattering efficiencies corre-

Received: May 12, 2015
Published: June 8, 2015

DOI: 10.1021/acsphotonics.5b00261
ACS Photonics 2015, 2, 993−999

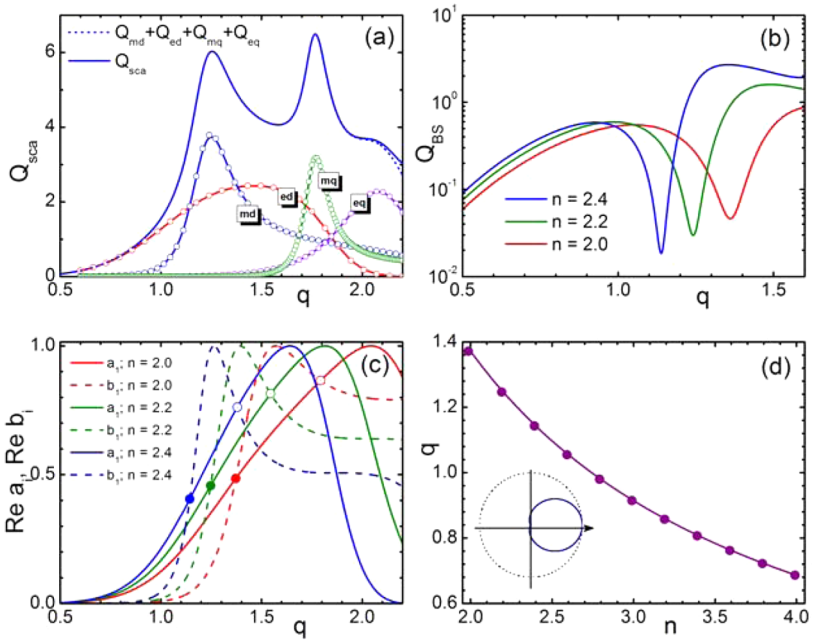

Figure 1. (a) Total scattering efficiency, Q_{sca}, vs size parameter $q = 2\pi R/\lambda$ for refractive index $n = 2.4$. Four partial scattering efficiencies (curves with open circles) corresponding to the electric dipole (ed), magnetic dipole (md), electric quadrupole (eq), and magnetic quadrupole (mq) contributions. (b) Backscattering efficiency Q_{BS} (in logarithmic scale) vs size parameter q for three different values of refractive index $n = 2.0$, 2.2, and 2.4, exhibiting a pronounced minima at particular values of size parameter. (c) Values of electric dipole coefficient a_1 (solid lines) and magnetic dipole coefficient b_1 (dashed lines). Positions in which $\mathrm{Re}a_1 = \mathrm{Re}b_1$ and $\mathrm{Im}a_1 = \mathrm{Im}b_1$, corresponding to the first Kerker condition,[9,10] are plotted as filled circles. The associated values of q correspond with high accuracy to the minimum values of Q_{BS}. For open circles one have $\mathrm{Re}a_1 = \mathrm{Re}b_1$ but $\mathrm{Im}a_1 = -\mathrm{Im}\ b_1$. (d) Trajectory of minimum back scattering on the plane of parameters $\{n,q\}$. Solid line presents solution to the equation $a_1 = b_1$, while circles are numerical solutions to the equation $Q_{BS} \rightarrow$ min. Inset in plot (d) shows polar scattering diagram[19] along the trajectory $Q_{BS} \rightarrow$ min with pronounced forward scattering.

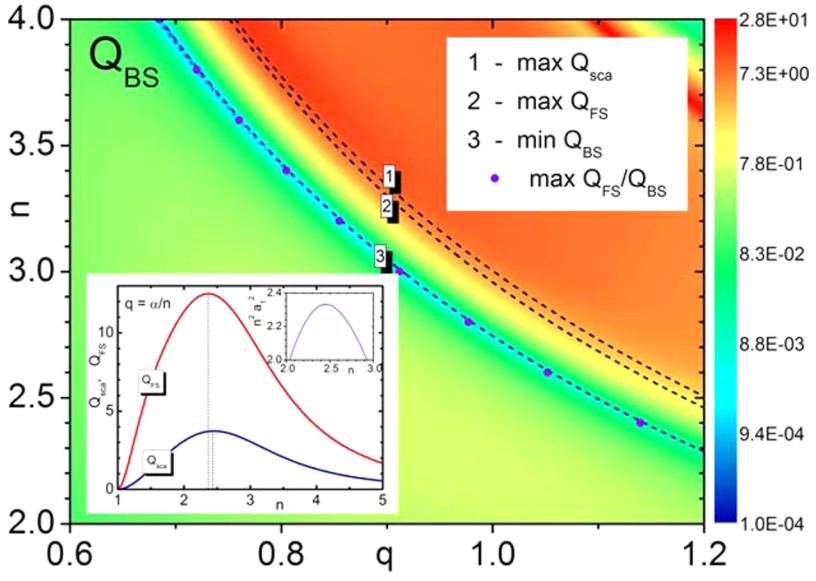

Figure 2. Contour plot of the backscattering efficiency $Q_{BS}(q,n)$ on the q,n parameters' plane. Dashed lines show trajectories of maximum total Q_{sca} (curve 1) and forward Q_{FS} (curve 2) scattering efficiencies. Curve 3 shows the trajectory of the minimum back scattering efficiency. Inset shows the variation of Q_{sca} and Q_{FS} along the trajectory $q = q(n)$, where Q_{BS} reaches minimum (i.e., along curve 3). The upper right part of the inset presents the function $|a_1(n)|^2 n^2$ along the trajectory of the first Kerker's condition.

sponding to $Q_1^{(e)}$, electric dipole (ed), $Q_1^{(m)}$, magnetic dipole (md), $Q_2^{(e)}$, electric quadrupole (eq), and $Q^{(m)}{}_2$, magnetic quadrupole (mq) are shown in Figure 1a for a sphere with $n = 2.4$. The total scattering efficiency can be accurately described in this range of q values as a sum of these four partial resonant efficiencies. The two observed dominant peaks can be identified with the resonant excitation of the magnetic dipolar and magnetic quadrupolar modes. We can also see pronounced minima in the backscattering cross sections depicted in Figure 1b. These minima correspond to the so-called "first Kerker's condition" $a_1 = b_1$, for which the amplitudes and phases of electric and magnetic dipoles are equal. This condition is

DOI: 10.1021/acsphotonics.5b00261
ACS Photonics 2015, 2, 993−999

marked by filled circles in Figure 1c. Satisfying the condition $a_1 = b_1$ for both real and imaginary part leads to the solution $nq = \alpha$ = const, where $\alpha \approx 2.7437$ is the root of the equation:

$$1 + (2\alpha^2 - 1)\cos(2\alpha) + \alpha(\alpha^2 - 2)\sin(2\alpha) = 0$$

which follows from equations (4)-(6) in Methods. In Figure 1d we present the trajectory of minimum backscattering on a q,n parameters' plane. From this figure one can conclude that minimum backscattering is well described by solution of $nq = \alpha$ not only for $q \ll 1$ (i.e., conventional condition for applicability of the dipole approximation) but even for values of size parameter q of the order of unity. The reason for this effect can be seen in Figure 1a for $n = 2.4$ and for a general case in Supporting Information, Figure 1S. Along the trajectory $q = \alpha/n$ and for a refractive index above 1.5 higher order modes (quadrupoles, etc.) are strongly suppressed compared to the dominant dipole modes.

In Figure 2, we show a contour plot of the backscattering cross-section where one can see the trajectory of the pronounced minimum of $Q_{BS}(n,q)$ (dashed curve 3). Trajectory of the maximum value of Q_{FS}/Q_{BS} (circles) practically coincides with curve 3. Additionally, trajectories of the maximum value of total scattering $Q_{sca}(n,q)$ (curve 1) and maximum forward scattering $Q_{FS}(n,q)$ (curve 2) are also shown in the figure. All these curves follow approximately hyperbolic dependence on the refractive index and, consequently, do not cross each other. This means that for a spherical particle, whatever the particle parameters are, it is not possible to obtain resonant values of the total $Q_{sca}(n,q)$ or forward $Q_{FS}(n,q)$ scattering efficiencies along the trajectory fulfilling the first Kerker's condition for the minimum backward scattering $a_1 = b_1$. From formula 2, see Methods, the latter condition leads to $Q_{FS} \propto |a_1|^2/q^2 \propto n^2|a_1|^2$, and therefore, the maximum value of Q_{FS} corresponds to the maximum value of $n^2|a_1|^2$ (see inset in Figure 2). However, the values of scattering amplitudes $|a_1| = |b_1|$ at maximum Q_{FS} are quite small, below 0.5 (see Figure 1c). It is clear that if we would be able to overlap electric and magnetic resonances at the point $a_1 = b_1 \approx 1$ we could enhance both total and forward scattering values.

One of the possibilities to satisfy condition $a_1 = b_1 \approx 1$ is to use metallic-dielectric core−shell nanoparticles.[20] It can also be reached by changing the particle's shape, for example, using oblate spheroidal nanoparticles instead of spheres. As it was shown in our previous work (see Figure 4 in ref 15), squeezing a silicon sphere into a spheroid with aspect ratio around 1:2, it is possible to obtain overlapping between the electric and magnetic dipole resonances and minimized backward scattering close to the wavelength of scattering resonances. This is also consistent with results published later for silicon nanodisks.[17] Going one step further, we will now demonstrate that for any given value of the particle refractive index there is a particular particle shape at which a resonant forward scattering with minimized backward scattering can be realized.

Solution of the wave equation in spheroidal coordinates can be made using the separation of variables method[21] (see also Methods). In the following we will focus our study on oblate spheroids, since for this shape electric and magnetic dipole resonances can be overlapped. An oblate spheroid (ellipsoid of revolution) is obtained by the rotation of an ellipse with focal distance d around its minor axis. The ratio of the major semiaxis a to the minor semiaxis b (i.e., the aspect ratio a/b) characterizes the particle shape, which may vary from a nearly spherical ($a/b \approx 1$) to a disk one ($a/b \gg 1$). The particle size can be specified by parameter $g = (2\pi/\lambda)(d/2)$ related to the length of the focal distance or by parameter $q_v = (2\pi r_v/\lambda)$, related to the radius of the sphere r_v whose volume is equal to that of the spheroid. For oblate spheroids, $r_v^3 = a^2b$. The connection between g and q_v is given by

$$q_v = g\frac{(a/b)^{2/3}}{[(a/b)^2 - 1]^{1/2}} = \frac{2\pi a}{\lambda}(a/b)^{-1/3}$$

where the size parameter $q = (2\pi a/\lambda)$ plays the same role as parameter $(2\pi R/\lambda)$ in the Mie theory.

In general, the angle β between the propagation direction and the rotation axis of the spheroid can be arbitrary ($0° \le \beta \le 90°$). Here, we study the case $\beta = 0$ when radiation propagates along the minor axis.

In Figure 3 we show the total $\tilde{Q}_{sca}$ and forward $\tilde{Q}_{FS}$ scattering efficiencies (see Methods for details) of oblate spheroidal

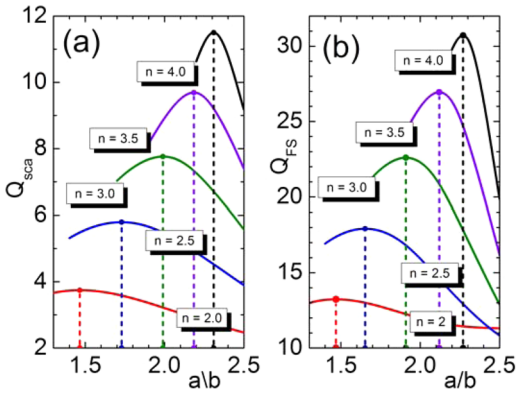

Figure 3. Variation of total $\tilde{Q}_{sca}$ (a) and forward $\tilde{Q}_{FS}$ (b) scattering efficiencies along the trajectories of minimum backward scattering for oblate spheroidal particles with different refractive index n vs aspect ratio a/b.

particles with different refractive index n versus aspect ratio a/b along the trajectories of minimum backward scattering. It can be seen from the figure that for each value of the particle refractive index there is an aspect ratio of the spheroid a/b for which the scattering efficiencies are optimized. As a general rule, higher values of scattering efficiencies can be achieved with higher refractive indices. This is not the case of spherical particles whose directional scattering is optimized at refractive index of ~2.45 (see inset in Figure 2). For each particular material one can find an optimum spheroidal shape that will produce a maximum forward scattering at a minimum back scattering.

One can compare the efficiency of forward scattering by spherical and spheroidal particles at the minimized back-scattering condition. For example, spherical particle with $n \approx 2.4$ has maximum forward scattering $Q_{FS} = \tilde{Q}_{FS} \approx 12.3$ (see inset in Figure 2). An optimized spheroidal particle with the same refractive index and $a/b \approx 1.7$ has about 1.4× higher forward scattering efficiency. With higher refractive index, this difference becomes much more pronounced. For a spherical particle with $n \approx 4$, one can reach maximum $\tilde{Q}_{FS} \approx 4$. An oblate particle with $n \approx 4$ and $a/b \approx 2.25$ permits to reach $\tilde{Q}_{FS}$ value above 30, with the back scattering close to zero. *This presents a huge interest for optical antennas.* Naturally, deformation of the particle shape leads also to some shift in the position of the resonant frequency.

DOI: 10.1021/acsphotonics.5b00261
ACS Photonics 2015, 2, 993−999

Final result of optimization is presented in Figure 4. It shows the dependence of the optimum shape of the spheroids on the

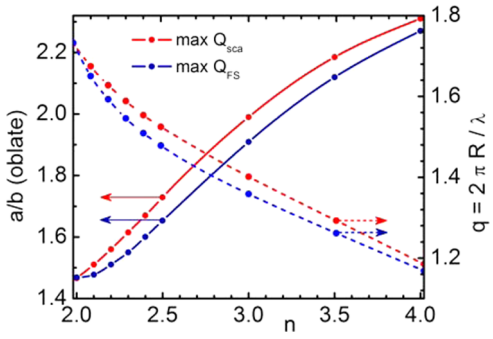

Figure 4. Optimum shape a/b (solid lines) and size parameter q (dashed lines) for spheroidal particles vs value of refractive index n.

particle refractive index: $a/b = f(n)$, which corresponds to maximum of $\tilde{Q}_{sca}$ or $\tilde{Q}_{FS}$ (solid lines) with minimized $\tilde{Q}_{BS}$. Resonant frequencies follow from the resonant values of the size parameter $q = q(n)$ related to these shapes (shown by corresponding dashed curves). For example, for $n = 3.5$, one can find from Figure 4 values $a/b \approx 2.09$ and $q \approx 1.28$ for optimum forward scattering.

As we mentioned above, the physical reason for scattering maximization is related to overlapping of magnetic and electric dipole resonances of the particles. Dynamics of this overlapping for particles with refractive index $n = 3.5$ is shown in Figure 5. For spherical particle $a/b = 1$ magnetic (md) and electric (ed) dipole resonances are well separated. It can be easily seen from the corresponding partial scattering efficiencies calculated from the Mie theory. Similar multipole decomposition for partial efficiencies can be done for spheroidal particles as well (see Methods for details). According to Figure 4, optimum condition for forward scattering is reached for $a/b = 2.086$. In Figure 5 one can see that with increase of the aspect ratio the electric and magnetic dipole resonances approach each other and fully merged at $a/b = 2.086$, which allows obtaining minimum backward scattering condition at the resonance of total scattering.

We would like to highlight that saying "electric dipole resonance" we mean the first electric dipole maximum for the smallest value of the size parameter. As it can be seen from Figure 5, other electric dipole maxima, even with higher intensity, appear at higher values of the size parameter. This electric dipole behavior is known for different dielectric nanoparticle shapes and is strongly affected by interference between the electric dipole and toroidal dipole, which has similar radiation pattern.[22]

Up to this point we have only considered lossless particles. Naturally, material absorption, in general, should influence both scattering diagram and near field intensity distribution. We estimated this influence from the Mie theory for spherical particles. For materials with a refractive index $n > 2$ and $\kappa \leq 0.05$ (typical for weakly dissipative materials), variations in scattering diagram are negligible (see Figure S2 in Supporting Information). For Si particles at IR range with $\lambda > 1$ μm dissipation practically does not influence scattering diagram.

Another important issue, with implications to a possible experimental realization, concerns the influence of a substrate, which is always necessary to support nanoparticles. There are two ways to support such a particle: (1) immerse it in

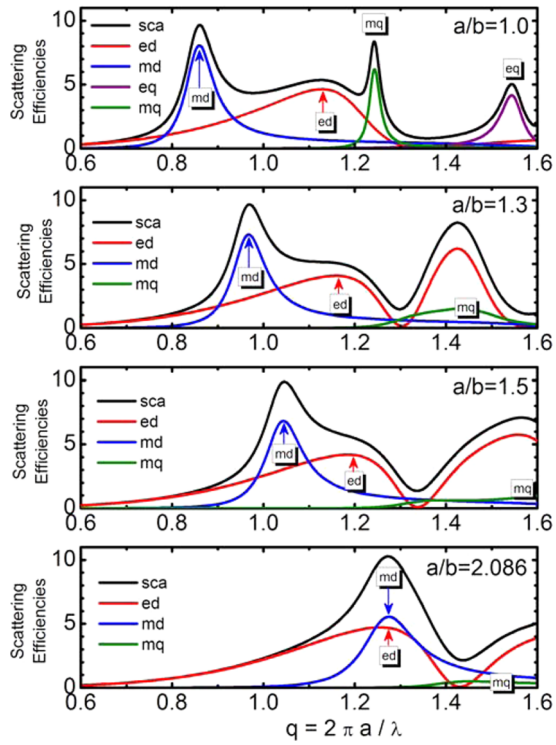

Figure 5. Overlapping of electric and magnetic dipole resonances for different particle shapes. Total scattering efficiency (black line), together with the corresponding electric $Q_1^{(e)}$ (red line) and magnetic $Q_1^{(m)}$ (blue line) scattering dipolar contributions are plotted vs size parameter q for different values of the aspect ratio a/b, ranging from 1 (sphere) to the optimized value 2.086. Green and purple curves plot the scattering contribution of the magnetic and electric quadrupole modes, respectively.

transparent materials with lower refractive index or (2) put it on a substrate. For spherical particles, the influence of surrounding media can be studied with the Mie theory. It shows that the electric dipole resonance is red-shifted and broadened (compared to particle in vacuum), while position of magnetic dipole resonance is less sensitive to the refractive index of the surrounding media, and only broadens. Thus, investigation of the Kerker resonance in this situation shows that the conditions for maximal forward scattering can still be met, with a red shift in the peak position and a broadening of the resonance. For spheroids, any detuning in the relative positions of electric and magnetic dipole resonances can be compensated by adjusting the geometrical aspect ratio. Some of the shape effects for metallic particles in different surrounding media were also investigated.[23]

For a particle on the surface, this problem also has an exact analytical solution.[24] The solution is valid for any incident angle. Investigation of the influence of the substrate based on the exact analytical solution was done for spherical plasmonic particles, for example, in ref 25. In this case, the electric dipole resonance also presents a red shift and broadening. Recently this problem was numerically investigated for the case of cylindrical dielectric nanoparticles.[26] This paper also demonstrates that effect of substrate is more pronounced for the electric resonance. Nevertheless, for spheroid, this effect can also be compensated by tuning the aspect ratio.

Although above we investigated only spheroidal nanoparticles, this is not the only shape for which the directional scattering effect can be achieved. It can be expected that all

DOI: 10.1021/acsphotonics.5b00261
ACS Photonics 2015, 2, 993−999

different types of geometries (e.g., cylinders, bricks, etc.) should have qualitatively similar variations of scattering properties versus nanoparticle shape. To prove this in Figure 6, we

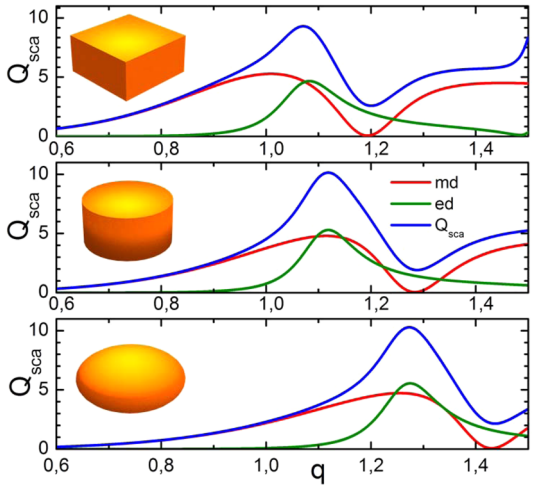

Figure 6. Scattering characteristics for parallelepiped (top panel), cylindrical (middle panel), and spheroid (bottom panel) particles with the same aspect ratio of 2.086 and refractive index $n = 3.5$. Scattering efficiencies of electric and magnetic dipoles obtained through multipole decomposition are shown by red and green lines, respectively. Scattering cross sections are normalized by the cross-section of the sphere with the volume equal to that of each nanoparticle.

additionally compared three different types of geometries (spheroids, cylinders, bricks) with the refractive index $n = 3.5$. It can be seen that the optimal aspect ratio and maximal scattering values are almost the same for all three shapes. The only difference is in the optimal resonance positions. Thus, from the analysis of spheroidal particles we can also understand the shape effect in the other geometries. The advantage of spheroids is a possibility to use analytical calculations based on exact solutions of Maxwell equations, while the other geometries require time-consuming numerical calculations.

In conclusion, we have investigated the problem of the shape optimization for oblate spheroidal dielectric particles aimed to obtain minimum backscattering together with maximized total and forward scattering. We have shown that this optimization is possible for any given value of refractive index. Such optimized particles are extremely efficient directional optical nano-antennas, which can act as Huygens sources.[11] Efficiency of spheroidal scatterers depends on the refractive index of the material and can be significantly higher than those which can be reached with spherical particles. These calculations also permit to understand the shape effect in the other practical geometries important from the experimental point of view (cylinders, blocks, etc.).

METHODS

Scattering by Spheres. Scattering efficiencies for total, Q_{sca}, forward, Q_{FS}, and backward, Q_{BS}, scattering of a spherical particle can be derived within the framework of Mie theory[18] and written as

$$Q_{sca} = \frac{2}{q^2}\sum_{l=1}^{\infty}(2l+1)(|a_l|^2 + |b_l|^2) \quad (1)$$

$$Q_{FS} = \frac{1}{q^2}\left|\sum_{l=1}^{\infty}(2l+1)(a_l + b_l)\right|^2 \quad (2)$$

$$Q_{BS} = \frac{1}{q^2}\left|\sum_{l=1}^{\infty}(2l+1)(-1)^l(a_l - b_l)\right|^2 \quad (3)$$

The electric, a_l, and magnetic, b_l, scattering amplitudes for nonmagnetic materials, and dielectric permittivity $\varepsilon = n^2$ (n being the refractive index of the particle material) are given by

$$a_l = \frac{\mathcal{R}_l^{(a)}}{\mathcal{R}_l^{(a)} + i\mathcal{T}_l^{(a)}},\ b_l = \frac{\mathcal{R}_l^{(b)}}{\mathcal{R}_l^{(b)} + i\mathcal{T}_l^{(b)}} \quad (4)$$

where $\mathcal{R}_l$ and $\mathcal{T}_l$ functions are defined as follows:

$$\mathcal{R}_l^{(a)} = n\psi_l'(q)\psi_l(nq) - \psi_l(q)\psi_l'(nq),$$
$$\mathcal{T}_l^{(a)} = n\chi_l'(q)\psi_l(nq) - \chi_l(q)\psi_l'(nq) \quad (5)$$

$$\mathcal{R}_l^{(b)} = n\psi_l'(nq)\psi_l(q) - \psi_l(nq)\psi_l'(q),$$
$$\mathcal{T}_l^{(b)} = n\chi_l(q)\psi_l'(nq) - \psi_l(nq)\chi_l'(q) \quad (6)$$

Here, $\psi_l(z) = \sqrt{\frac{\pi z}{2}}J_{l+1/2}(z)$, $\chi_l(z) = \sqrt{\frac{\pi z}{2}}N_{l+1/2}(z)$, where $J_{l+1/2}(z)$ and $N_{l+1/2}(z)$ are the Bessel and Neumann functions. The radius of the particle R enters in this theory through the dimensionless size parameter $q = \omega R/c = 2\pi R/\lambda$, where ω is the angular frequency, c the speed of light, and λ the radiation wavelength in vacuum. The prime in formulas 5 and 6 indicates differentiation with respect to the argument of the function, that is, $\psi_l'(z) \equiv d\psi_l(z)/dz$, and so on. The efficiencies (1)−(3) represent the corresponding cross sections normalized to the geometrical cross section of the sphere. The total scattering efficiency is then given by the sum of partial scattering efficiencies:

$$Q_{sca} = \sum_{l=1}^{\infty}(Q_l^{(e)} + Q_l^{(m)}) \quad (7)$$

where each partial efficiency corresponds to the radiation of the l-th order multipole. Terms $Q_l^{(e)}$ and $Q_l^{(m)}$ describe the radiation related to the electric and magnetic polarizabilities, respectively. We consider transparent dielectrics with $\mathrm{Im}\varepsilon = 0$, so $Q_{ext} = Q_{sca}$.

Scattering by Spheroids. The optical properties of spheroidal particles can be determined by various methods of light scattering theory. Most frequently, the separation of variables method and the T-matrix method are used. The survey of methods can be found in ref 27 (see also Database of Optical Properties of cosmic dust analogues, DOP, http://www.astro.spbu.ru/DOP/3-REVS/index.html).

Asano and Yamamoto[28] obtained the first solution to the light scattering problem for spheroids with a complex refractive index. The method is based on the solution to the Helmholtz equation in the spheroidal coordinate system. Asano and Yamamoto applied the Debye potentials to describe the electromagnetic fields, which is similar to the Mie solution for spheres. The scattering coefficients then are found in the infinite systems of the linear algebraic equations and can be found by solving truncated systems.

DOI: 10.1021/acsphotonics.5b00261
ACS Photonics 2015, 2, 993−999

Another solution was published by Farafonov[29] (see ref 30 for first numerical results). Its principal distinction from the previous one is the special basis for the representation of the electromagnetic fields, a combination of the Debye and Hertz potentials (i.e., the potentials introduced to solve the light scattering problem for spheres and infinitely long cylinders, respectively). The approach has an incontestable advantage for strongly elongated or flattened particles.

In this paper, we use the most recent version of the numerical code based on the Farafonov's solution (see http://www.astro.spbu.ru/DOP/6-SOFT/SPHEROID/1-SPH_new/). The comparison of methods and benchmark results can be found in ref 31.

For spheroids, one usually calculates the scattering efficiency factors $Q = \sigma/S$, which are the ratios of the corresponding cross sections σ to the geometrical cross-section S of the spheroid (the area of the particle's shadow). For oblate spheroids and $\beta = 0$, $S = \pi a^2$. The efficiencies for forward, Q_{FS}, and backward, Q_{BS}, scattering are[32] (pay attention that eq 5.80 for back-scattering efficiency in ref 32, p. 137 must be corrected):

$$Q_{FS} = \frac{1}{q_v^2 (a/b)^{2/3}} \left| \sum_{l=1}^{\infty} i^{-l} b_l^{(1)} \sum_{r=0,1}^{\infty}{}' d_r^{1l}(-ig)(r+1)(r+2) \right|^2 \tag{8}$$

$$Q_{BS} = \frac{1}{q_v^2 (a/b)^{2/3}} \left| \sum_{l=1}^{\infty} i^{l} b_l^{(1)} \sum_{r=0,1}^{\infty}{}' d_r^{1l}(-ig)(r+1)(r+2) \right|^2 \tag{9}$$

Here, $b_l^{(1)}$ are the coefficients for scattered radiation, which are determined from the solution to the light scattering problem, and $d_r^{1l}(-ig)$ are the expansion coefficients of oblate angular spheroidal functions in terms of associated Legendre polynomials. The prime over the summation symbols indicates the even (odd) terms only are summarized when the index $(l-1)$ is even (odd).

A convenient way to compare the optical properties of particles with different shapes is normalizing the cross sections by the geometrical cross sections of the equal volume spheres, $\sigma/\pi r_v^2$. For oblate spheroids and $\beta = 0°$, we have

$$\tilde{Q} = \frac{\sigma}{\pi r_v^2} = (a/b)^{2/3} Q \tag{10}$$

We note that the case of $\beta \neq 0$ is also very interesting due to the appearance of additional, azimuthally nonsymmetric modes.[33] This study, being much more involved, would however obscure the simplicity of the present results and deserve, in our opinion, a separate publication.

Multipole Decomposition. Multipole decomposition allows one to identify the multipolar character of the different resonances being excited in a system.[34−36] In our case, it was performed by projecting the electromagnetic field scattered by the spheroids into the Vector Spherical Harmonics basis on a spherical surface with radius R_0 enclosing the structure. The center of the sphere was chosen to coincide with the center of the spheroid. In this way, one can compute the electric a_{lm} and magnetic b_{lm} scattering coefficients associated with a certain multipolar contribution as

$$a_{lm} = \frac{(-i)^{l+1} kR_0}{h_l^{(1)}(kR_0)[\pi(2l+1)l(l+1)]^{1/2} E_0} \iint Y_{lm}^*(\theta, \phi)\hat{r}\cdot E_{sca}\,d\Omega \tag{11}$$

$$b_{lm} = \frac{\eta(-i)^{l} kR_0}{h_l^{(1)}(kR_0)[\pi(2l+1)l(l+1)]^{1/2} E_0} \iint Y_{lm}^*(\theta, \phi)\hat{r}\cdot H_{sca}\,d\Omega \tag{12}$$

where $h_l^{(1)}(kR_0)$ is the spherical Hankel function of first kind and order l, E_0 is the amplitude of the incident field, the scattered fields are projected into a radial unitary vector and:

$$Y_{lm}(\theta, \phi) = \sqrt{\frac{2l+1}{4\pi}\frac{(l-m)!}{(l+m)!}} P_l^m(\cos\theta) e^{im\phi} \tag{13}$$

with $P_l^m(\cos\theta)$ being the associated Legendre polynomials. The partial scattering efficiency due to the l-th electric or magnetic multipole can then be computed as

$$Q_l^E = \frac{2l+1}{q^2} \sum_{m=-l}^{l} |a_{lm}|^2 \tag{14}$$

$$Q_l^M = \frac{2l+1}{q^2} \sum_{m=-l}^{l} |b_{lm}|^2 \tag{15}$$

Q or $\tilde{Q}$ is obtained depending on whether one uses q or q_v. The total scattering efficiency can be retrieved by summing up the contributions of the different electric and magnetic multipoles. While the choice of the radius of the sphere is arbitrary, the only requirement to achieve accurate results is a sufficiently accurate angular resolution in the integral.

■ ASSOCIATED CONTENT

Supporting Information

(S1) An additional figure showing the variation of quadrupole mode amplitudes a_2 and b_2 versus refractive index along the trajectory of Kerker's condition. (S2) An additional figure showing the dependence of the scattering diagram on the dissipation parameter. The Supporting Information is available free of charge on the ACS Publications website at DOI: 10.1021/acsphotonics.5b00261.

■ AUTHOR INFORMATION

Corresponding Author

*E-mail: boris_l@dsi.a-star.edu.sg.

Notes

The authors declare no competing financial interest.

■ ACKNOWLEDGMENTS

This work was supported by Data Storage Institute (DSI) core funds. N.V.V. acknowledges the support from RFBR grant 13-02-00138a.

■ REFERENCES

(1) Novotny, L.; Hecht, B. *Principles of nano-optics*. Cambridge University Press: New York, 2006.

(2) Evlyukhin, A. B.; Reinhardt, C.; Seidel, A.; Luk'yanchuk, B. S.; Chichkov, B. N. Optical response features of Si-nanoparticle arrays. *Phys. Rev. B* **2010**, *82*, 045404.

(3) García-Etxarri, A.; Gómez-Medina, R.; Froufe-Pérez, L. S.; López, C.; Chantada, L.; Scheffold, F.; Aizpurua, J.; Nieto-Vesperinas, M.; Saénz, J. J. Strong magnetic response of submicron silicon particles in the infrared. *Opt. Express* **2011**, *19*, 4815−4826.

(4) Kuznetsov, A. I.; Miroshnichenko, A. E.; Fu, Y. H.; Zhang, J. B.; Luk'yanchuk, B. Magnetic light. *Sci. Rep.* **2012**, *2*, 492.

(5) Evlyukhin, A. B.; Novikov, S. M.; Zywietz, U.; Eriksen, R. L.; Reinhardt, C.; Bozhevolnyi, S. I.; Chichkov, B. N. Demonstration of

DOI: 10.1021/acsphotonics.5b00261
ACS Photonics 2015, 2, 993−999

magnetic dipole resonances of dielectric nanospheres in the visible region. *Nano Lett.* **2012**, *12*, 3749−3755.
(6) Ginn, J. C.; Brener, I.; Peters, D. W.; Wendt, J. R.; Stevens, J. O.; Hines, P. F.; Basilio, L. I.; Warne, L. K.; Ihlefeld, J. F.; Clem, P. G.; Sinclair, M. B. Realizing optical magnetism from dielectric metamaterials. *Phys. Rev. Lett.* **2012**, *108*, 097402.
(7) Schuller, J. A.; Zia, R.; Taubner, T.; Brongersma, M. L. Dielectric metamaterials based on electric and magnetic resonances of silicon carbide particles. *Phys. Rev. Lett.* **2007**, *99*, 107401.
(8) Shi, L.; Harris, J. T.; Fenollosa, R.; Rodríguez, I.; Lu, X.; Korgel, B. A.; Meseguer, F. Monodisperse silicon nanocavities and photonic crystals with magnetic response in the optical region. *Nat. Commun.* **2013**, *4*, 1904.
(9) Kerker, M.; Wang, D.-S.; Giles, C.-L. Electromagnetic scattering by magnetic spheres. *J. Opt. Soc. Am.* **1983**, *73*, 765−767.
(10) Nieto-Vesperinas, M.; Gómez-Medina, R.; Saénz, J. J. Angle-suppressed scattering and optical forces on submicrometer dielectric particles. *J. Opt. Soc. Am. A* **2011**, *28*, 54−60.
(11) Krasnok, A. E.; Miroshnichenko, A. E.; Belov, P. A.; Kivshar, Y. S. All-dielectric optical nanoantennas. *Opt. Express* **2012**, *20*, 20599−20604.
(12) Rolly, B.; Stout, B.; Bonod, N. Boosting the directivity of optical antennas with magnetic and electric dipolar resonant particles. *Opt. Express* **2012**, *20*, 20376−20386.
(13) Albella, P.; Poyli, M. A.; Schmidt, M. K.; Maier, S. A.; Moreno, F.; Saénz, J. J.; Aizpurua, J. Low-loss electric and magnetic field-enhanced spectroscopy with subwavelength silicon dimers. *J. Phys. Chem. C* **2013**, *117*, 13573−13584.
(14) Geffrin, J. M.; García-Cámara, B.; Gómez-Medina, R.; Albella, P.; Froufe-Pérez, L. S.; Eyraud, C.; Litman, A.; Vaillon, R.; González, F.; Nieto-Vesperinas, M.; Sáenz, J. J.; Moreno, F. Magnetic and electric coherence in forward- and back-scattered electromagnetic waves by a single dielectric subwavelength sphere. *Nat. Commun.* **2012**, *3*, 1171.
(15) Fu, Y. H.; Kuznetsov, A. I.; Miroshnichenko, A. E.; Yu, Y. F.; Luk'yanchuk, B. Directional visible light scattering by silicon nanoparticles. *Nat. Commun.* **2013**, *4*, 1527.
(16) Person, S.; Jain, M.; Lapin, Z.; Sáenz, J. J.; Wicks, G.; Novotny, L. Demonstration of zero optical backscattering from single nanoparticles. *Nano Lett.* **2013**, *13*, 1806−1809.
(17) Staude, I.; Miroshnichenko, A. E.; Decker, M.; Fofang, N. T.; Liu, S.; Gonzales, E.; Dominguez, J.; Luk, T. S.; Neshev, D. N.; Brener, I.; Kivshar, Y. Tailoring directional scattering through magnetic and electric resonances in subwavelength silicon nanodisks. *ACS Nano* **2013**, *7*, 7824−7832.
(18) Bohren, C. F.; Huffman, D. R. *Absorption and Scattering of Light by Small Particles*; Wiley: New York, 1998.
(19) Born, M.; Wolf, E. *Principles of Optics*, 7th ed., University Press: Cambridge, 1999.
(20) Liu, W.; Miroshnichenko, A. E.; Neshev, D. N.; Kivshar, Y. S. Broadband unidirectional scattering by magneto-electric core-shell nanoparticles. *ACS Nano* **2012**, *6*, 5489−5497.
(21) Voshchinnikov, N. V.; Farafonov, V. G. Optical properties of spheroidal particles. *Astrophys. Space Sci.* **1993**, *204*, 19−86.
(22) Miroshnichenko, A. E.; Evlyukhin, A. B.; Yu, Y. F.; Bakker, R. M.; Chipouline, A.; Kuznetsov, A. I.; Luk'yanchuk, B.; Chichkov, B. N.; Kivshar, Y. S. Seeing the unseen: observation of an anapole with dielectric nanoparticles. *ArXiv:1412.0299* **2014**.
(23) Kelly, K. L.; Coronado, E.; Zhao, L. L.; Schatz, G. C. The optical properties of metal nanoparticles: The influence of size, shape, and dielectric environment. *J. Phys. Chem. B* **2003**, *107*, 668−677.
(24) Bedeaux, B.; Vlieger, J. *Optical properties of surfaces*, 2nd ed.; Imperial College Press: London, 2004.
(25) Luk'yanchuk, B. S.; Zheng, Y. W.; Lu, Y. F. Laser cleaning of solid surface: Optical resonance and near-field effects. *Proc. SPIE* **2000**, *4065*, 576−587.
(26) Evlyukhin, A. B.; Eriksen, R. L.; Cheng, W.; Beermann, J.; Reinhardt, C.; Petrov, A.; Prorok, S.; Eich, M.; Chichkov, B. N.; Bozhevolnyi, S. I. Optical spectroscopy of single Si nanocylinders with magnetic and electric resonances. *Sci. Rep.* **2014**, *4*, 4126−4130.
(27) Mishchenko, M. I., Hovenier, J., Travis, L. D., Eds. *Light Scattering by Nonspherical Particles*; Academic Press: San Francisco, 2000.
(28) Asano, S.; Yamamoto, G. Light scattering by a spheroidal particle. *Appl. Opt.* **1975**, *14*, 29−49.
(29) Farafonov, V. G. The scattering of a plane electromagnetic wave by a dielectric spheroid. *Differ. Equations* **1983**, *19*, 1765−1777.
(30) Voshchinnikov, N. V.; Farafonov, V. G. Light scattering by dielectric spheroids. I. *Opt. Spektrosc.* **1985**, *58*, 81−85.
(31) Voshchinnikov, N. V.; Il'in, V. B.; Henning, Th.; Michel, B.; Farafonov, V. G. Extinction and polarization of radiation by absorbing spheroids: Shape/size effects and some benchmarks. *J. Quant. Spectrosc. Radiat. Transfer* **2000**, *65*, 877−893.
(32) Farafonov, V. G. Application of non-orthogonal bases in the theory of light scattering by spheroidal particles. *Light Scattering Reviews*; Springer-Praxis: New York, 2013; Vol. *8*, pp 189−268.
(33) Krasnok, A. E.; Simovski, C. R.; Belov, P. A.; Kivshar, Y. S. Superdirective dielectric nanoantennas. *Nanoscale* **2014**, *6*, 7354−7361.
(34) Mühlig, S.; Menzel, C.; Rockstuhl, C.; Lederer, F. Multipole analysis of meta-atoms. *Metamaterials* **2011**, *5*, 64−73.
(35) Grahn, P.; Shevchenko, A.; Kaivola, M. Electromagnetic multipole theory for optical nanomaterials. *New J. Phys.* **2012**, *14*, 093033.
(36) Kuznetsov, A. I.; Miroshnichenko, A. E.; Fu, Y. H.; Viswanathan, V.; Rahmani, M.; Valuckas, V.; Pan, Z. Y.; Kivshar, Y.; Pickard, D. S.; Luk'yanchuk, B. Split-ball resonator as a three-dimensional analogue of planar split-rings. *Nat. Commun.* **2014**, *5*, 3104.

DOI: 10.1021/acsphotonics.5b00261
ACS Photonics 2015, 2, 993−999